ELSEVIER

Thin-Walled Structures 38 (2000) 267–283

THIN-WALLED STRUCTURES

www.elsevier.com/locate/tws

Dynamic buckling of thin isotropic plates subjected to in-plane impact

D. Petry *, G. Fahlbusch

Universität der Bundeswehr München, Institut für Luftfahrttechnik und Leichtbau, D-85579 Neubiberg, Germany

Received 21 March 2000; accepted 31 August 2000

Abstract

The dynamic stability behaviour of imperfect simply supported plates subjected to in-plane pulse loading is investigated. For the calculation of dynamic buckling loads a stress failure criterion is applied. The large-deflection plate equations are solved by a Galerkin method by using Navier's double Fourier series. In this paper the dynamic load factor (DLF) is redefined and plots that are useful for the design of plate structures are presented. Parametric studies are performed in which the influences of the pulse duration, shock function, imperfection, geometric dimensions and limit stress of the material are discussed. Comparison between the dynamic buckling loads, which are obtained by the commonly used criterion of Budiansky and Hutchinson [Proceedings of the 11th International Congress of Applied Mechanics (1964) 636], and the dynamic elastic limit loads, which are computed by the stress failure criterion, shows that the latter criterion is more useful for the design of lightweight structures.

Keywords: Dynamic buckling; Plates; In-plane impact; Stress failure; Galerkin method

1. Introduction

The dynamic buckling analysis of in-plane loaded structures is a problem of dynamic response, in which imperfections are necessary to cause out-of-plane motion.

For those configurations that have an instable postbuckling branch (i.e., cylindrical

* Corresponding author. Tel.: +49-89-6004-4139; fax: +49-89-6004-4103.
E-mail address: dirk.petry@unibw-muenchen.de (D. Petry).

0263-8231/01/$ - see front matter
PII: S0263-8231(00)00037-9

shells), critical conditions for defining a dynamic buckling load can be found by using the Equation of Motion Approach or Energy Approaches [2]. But there does not exist any standard criterion for the investigation of structures with stable postbuckling behaviour like plates. Therefore it is necessary to establish critical conditions for finding a dynamic buckling load.

In different publications [3–5] dynamic buckling loads are determined by considering the stability criterion of Budiansky and Hutchinson [1]: a dynamically critical condition is defined if some characteristic value increases rapidly with the loading amplitude. In these works the quotient of the dynamic buckling load and the load of bifurcation is defined as the dynamic load-amplification factor (DLF). The disadvantage of this criterion is caused by the fact that the load-carrying capacity of the structure is not taken into account. Therefore such a criterion is not very useful for proper design of structures with a stable postbuckling branch.

In this paper the dynamic buckling of plates is investigated by using a stress failure criterion and the effects of the shock function, imperfections, geometric dimensions and limit stress of the material are studied.

2. Dynamic stability of plates

As will be shown in the following, the application of the Budiansky–Hutchinson criterion [1] leads to very conservative dynamic buckling loads. Therefore a dynamic buckling criterion that is founded on stress analysis is used: a stress failure occurs if the effective stress σ_E exceeds the limit stress σ_L of the material. A dynamic response caused by an impact is defined to be dynamically stable if

$$\sigma_E \leq \sigma_L \tag{1}$$

is fulfilled at every time everywhere in the structure. Even if local yielding does not result in global failure of the structure, it is practical for ductile materials to use the yield stress σ_Y as limit stress σ_L. The application of this stress failure criterion results in a unique failure load depending on the shock function. The corresponding amplitude of the impact function is called the dynamic failure load, N_F^{dyn}.

A dynamic load factor has been defined in the literature as the quotient of the dynamic buckling (here: failure) load, N_F^{dyn}, and the classical bifurcation load, N_{crit}:

$$\mathrm{DLF}_{crit} = \frac{N_F^{dyn}}{N_{crit}}. \tag{2}$$

Considering the fact that the static failure load of a plate could exceed its static bifurcation load several times [6], it seems better to compare the dynamic failure load N_F^{dyn} with the static one, N_F^{stat}. In redefining the dynamic load factor by

$$\mathrm{DLF} = \frac{N_F^{dyn}}{N_F^{stat}}, \tag{3}$$

this load-amplifying quotient only describes the dynamic behaviour of the structure under impact loading.

3. Analysis

Consider a rectangular plate of length a, width b and constant thickness h subjected to pulse loading $\bar{N}_x(t)$, $\bar{N}_y(t)$ and $\bar{N}_{xy}(t)$ (Fig. 1). The plate has an initial imperfection w_0 in the z-direction. The total transverse displacement is defined by

$$w = w_{el} + w_0, \tag{4}$$

where w_{el} is the flexible displacement. Applying Kirchhoff's hypothesis, the in-plane displacements $\bar{u}$ and $\bar{v}$ are taken as

$$\bar{u} = u(x, y) - z\frac{\partial w}{\partial x} \tag{5}$$

and

$$\bar{v} = v(x, y) - z\frac{\partial w}{\partial y}. \tag{6}$$

The derivatives of the displacements $\bar{u}$ and $\bar{v}$ — i.e., $\partial\bar{u}/\partial x$, $\partial\bar{u}/\partial y$, $\partial\bar{v}/\partial x$ and $\partial\bar{v}/\partial y$ — are small compared with $\partial w/\partial x$ and $\partial w/\partial y$. Accordingly, their squares are negligible against the other terms in the non-linear strain–displacement relations. Considering the imperfection they can be written as [7]:

$$\bar{\varepsilon}_x = \frac{\partial\bar{u}}{\partial x} + \frac{1}{2}\left(\frac{\partial w}{\partial x}\right)^2 - \frac{1}{2}\left(\frac{\partial w_0}{\partial x}\right)^2, \tag{7}$$

$$\bar{\varepsilon}_y = \frac{\partial\bar{v}}{\partial y} + \frac{1}{2}\left(\frac{\partial w}{\partial y}\right)^2 - \frac{1}{2}\left(\frac{\partial w_0}{\partial y}\right)^2 \tag{8}$$

and

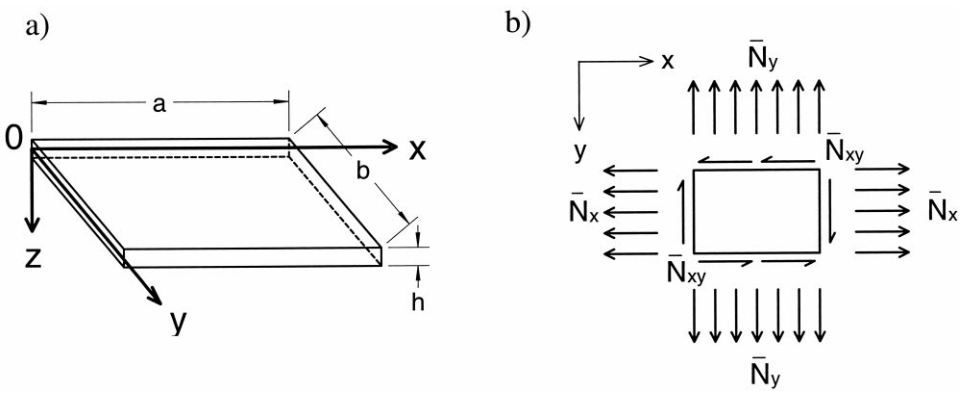

Fig. 1. (a) Plate dimensions and coordinates; (b) definition of the average boundary membrane forces.

$$\bar{\gamma}_{xy}=\frac{\partial \bar{u}}{\partial y}+\frac{\partial \bar{v}}{\partial x}+\frac{\partial w}{\partial x}\frac{\partial w}{\partial y}-\frac{\partial w_0}{\partial x}\frac{\partial w_0}{\partial y}. \tag{9}$$

As in the classic plate theory, the membrane forces N_x, N_y, N_{xy} and bending or twisting moments M_x, M_y, M_{xy} are defined by

$$\{N_x, N_y, N_{xy}\}=\int_{-h/2}^{+h/2}\{\sigma_x, \sigma_y, \tau_{xy}\}\,\mathrm{d}z \tag{10}$$

and

$$\{M_x, M_y, M_{xy}\}=\int_{-h/2}^{+h/2} z\{\sigma_x, \sigma_y, \tau_{xy}\}\,\mathrm{d}z. \tag{11}$$

Substituting the linear elastic Hooke's law for isotropic materials

$$\begin{Bmatrix}\sigma_x\\ \sigma_y\\ \tau_{xy}\end{Bmatrix}=\frac{E}{1-\nu^2}\begin{bmatrix}1 & \nu & 0\\ \nu & 1 & 0\\ 0 & 0 & \frac{1-\nu}{2}\end{bmatrix}\begin{Bmatrix}\bar{\varepsilon}_x\\ \bar{\varepsilon}_y\\ \bar{\gamma}_{xy}\end{Bmatrix} \tag{12}$$

into Eqs. (10) and (11), the membrane forces and the moments in terms of the three displacements can be derived. In Eq. (12), E is Young's modulus and ν is Poisson's ratio. Neglecting the terms of plane and rotary inertia, the applied strain–displacement relations lead to the following equation of motion

$$\rho h\ddot{w}=N_x\frac{\partial^2 w}{\partial x^2}+N_y\frac{\partial^2 w}{\partial y^2}+2N_{xy}\frac{\partial^2 w}{\partial x\partial y}-K(\Delta\Delta w-\Delta\Delta w_0)+q_z, \tag{13}$$

where Δ is the Laplacian operator, q_z is the load per area in the z-direction and the plate stiffness K is defined by

$$K=\frac{Eh^3}{12(1-\nu^2)}. \tag{14}$$

By combining the middle-plane strains $\varepsilon_x=\bar{\varepsilon}_x(z=0)$, $\varepsilon_y=\bar{\varepsilon}_y(z=0)$ and $\gamma_{xy}=\bar{\gamma}_{xy}(z=0)$, the compatibility equation

$$\frac{\partial^2\varepsilon_x}{\partial y^2}+\frac{\partial^2\varepsilon_y}{\partial x^2}-\frac{\partial^2\gamma_{xy}}{\partial x\partial x}=\left(\frac{\partial^2 w}{\partial x\partial y}\right)^2-\frac{\partial^2 w}{\partial x^2}\frac{\partial^2 w}{\partial y^2}-\left\{\left(\frac{\partial^2 w_0}{\partial x\partial y}\right)^2-\frac{\partial^2 w_0}{\partial x^2}\frac{\partial^2 w_0}{\partial y^2}\right\} \tag{15}$$

can be found. Regarding the definitions of membrane forces, by introducing Airy's stress function ϕ which satisfies

$$N_x=\frac{\partial^2\phi}{\partial y^2},\ N_y=\frac{\partial^2\phi}{\partial x^2}\ \text{and}\ N_{xy}=-\frac{\partial^2\phi}{\partial x\partial y}, \tag{16}$$

it follows that

$$\Delta\Delta\Phi=Eh\left[\left(\frac{\partial^2 w}{\partial x\partial y}\right)^2-\frac{\partial^2 w}{\partial x^2}\frac{\partial^2 w}{\partial y^2}-\left\{\left(\frac{\partial^2 w_0}{\partial x\partial y}\right)^2-\frac{\partial^2\omega_0}{\partial x^2}\frac{\partial^2 w_0}{\partial y^2}\right\}\right]. \tag{17}$$

This non-linear equation of compatibility takes the plane problem into consideration.

4. Solution of the plate equations

The boundary conditions for w and w_0 of a simply supported plate where the edges remain straight after buckling are:

$$\left.\begin{aligned} w=w_0=0\\ \frac{\partial^2 w}{\partial x^2}=\frac{\partial^2 w_0}{\partial x^2}=0\\ \frac{\partial u}{\partial y}=C_1\end{aligned}\right\}\ \text{at } x=0,\ a;\quad \left.\begin{aligned} w=w_0=0\\ \frac{\partial^2 w}{\partial y^2}=\frac{\partial^2 w_0}{\partial y^2}=0\\ \frac{\partial v}{\partial x}=C_2\end{aligned}\right\}\ \text{at } y=0,\ b. \tag{18}$$

If $\bar{N}_x$, $\bar{N}_y$ and $\bar{N}_{xy}$ are the average membrane forces at the edges, the stress function has to satisfy the following relations:

$$x=0,\ a:\quad \frac{1}{b}\int_0^b\frac{\partial^2\phi}{\partial y^2}\,dy=\bar{N}_x;\quad -\frac{1}{b}\int_0^b\frac{\partial^2\phi}{\partial x\partial y}\,dy=\bar{N}_{xy} \tag{19}$$

and

$$y=0,\ b:\quad \frac{1}{a}\int_0^a\frac{\partial^2\phi}{\partial x^2}\,dx=\bar{N}_y;\quad -\frac{1}{a}\int_0^a\frac{\partial^2\phi}{\partial x\partial y}\,dx=\bar{N}_{xy}. \tag{20}$$

In accordance with the boundary conditions, Navier's double Fourier series with the coefficients ${}^tW_{mn}$ and ${}^0W_{mn}$ are chosen to describe the displacement function $w(x, y)$ and the geometric imperfection $w_0(x, y)$:

$$w=\sum_{m=1}^{k}\sum_{n=1}^{l}{}^tW_{mn}\sin\frac{m\pi x}{a}\sin\frac{n\pi y}{b} \tag{21}$$

and

$$w_0=\sum_{m=1}^{k}\sum_{n=1}^{l}{}^0W_{mn}\sin\frac{m\pi x}{a}\sin\frac{n\pi y}{b}. \tag{22}$$

By inserting these two relations into the differential equation of compatibility [Eq. (17)] the following equation is obtained:

$$\Delta\Delta\Phi = Eh\left\{\sum_{i=1}^{k}\sum_{j=1}^{l}\sum_{m=1}^{k}\sum_{n=1}^{l}\left(\frac{ijmn\pi^4}{a^2b^2}\cos\frac{i\pi x}{a}\cos\frac{j\pi y}{b}\cos\frac{m\pi x}{a}\cos\frac{n\pi y}{b}\right.\right. \tag{23}$$

$$\left.\left.-\frac{i^2n^2\pi^4}{a^2b^2}\sin\frac{i\pi x}{a}\sin\frac{j\pi y}{b}\sin\frac{m\pi x}{a}\sin\frac{n\pi y}{b}\right)[{}^tW_{ij}\,{}^tW_{mn}-{}^0W_{ij}\,{}^0W_{mn}]\right\}.$$

Using different trigonometric relations, Airy's stress function can be derived as:

$$\Phi=\frac{1}{2}\bar{N}_x y^2+\frac{1}{2}\bar{N}_y x^2-\bar{N}_{xy}xy+Eh\sum_{i=1}^{k}\sum_{j=1}^{l}\left(A_1^{ij}\cos\frac{2i\pi x}{a}+A_2^{ij}\cos\frac{2j\pi y}{b}\right)[{}^tW_{ij}^2$$

$$-{}^0W_{ij}^2]+Eh\sum_{i=1}^{k}\sum_{j=1}^{l}\sum_{m=1}^{k}\sum_{n=1}^{l}{}^{(i,j)\neq(m,n)}\left\{A_3^{ijmn}\cos\frac{(i-m)\pi x}{a}\cos\frac{(j-n)\pi y}{b}\right.$$

$$+A_4^{ijmn}\cos\frac{(i-m)\pi x}{a}\cos\frac{(j+n)\pi y}{b}+A_5^{ijmn}\cos\frac{(i+m)\pi x}{a}\cos\frac{(j-n)\pi y}{b}$$

$$\left.+A_6^{ijmn}\cos\frac{(i+m)\pi x}{a}\cos\frac{(j+n)\pi y}{b}\right\}[{}^tW_{ij}\,{}^tW_{mn}-{}^0W_{ij}\,{}^0W_{mn}], \tag{24}$$

with the shortenings:

$$A_1^{ij}=\frac{a^2j^2}{32b^2i^2},\ A_3^{ijmn}=\frac{(ijmn-i^2n^2)a^2b^2}{4[(i-m)^2b^2+(j-n)^2a^2]^2},\ A_5^{ijmn}=\frac{(ijmn+i^2n^2)a^2b^2}{4[(i+m)^2b^2+(j-n)^2a^2]^2}$$

$$A_2^{ij}=\frac{b^2i^2}{32a^2j^2},\ A_4^{ijmn}=\frac{(ijmn+i^2n^2)a^2b^2}{4[(i-m)^2b^2+(j+n)^2a^2]^2},\ A_6^{ijmn}=\frac{(ijmn-i^2n^2)a^2b^2}{4[(i+m)^2b^2+(j+n)^2a^2]^2}.$$

With the definitions (16), the membrane forces N_x, N_y and N_{xy} are computable by this solution of ϕ and the boundary conditions (19) and (20) are satisfied. By using Eqs. (7, 8) and (12) one can show that the boundary conditions $\partial u/\partial y|_{x=0,\,a}$ and $\partial v/\partial x|_{y=0,\,b}$ [Eq. (18)] are valid too. Together with the double Fourier series [Eqs. (21) and (22)] the membrane forces are inserted into the equation of motion [Eq. (13)]. The relation obtained is multiplied by

$$\sin\frac{r\pi x}{a}\sin\frac{s\pi y}{b},\quad r=1,2,\ldots,k;\ s=1,2,\ldots,l \tag{25}$$

and next integrated over the plate area. A system of $k\times l$ second-order ordinary differential equations is obtained to compute the coefficients ${}^tW_{rs}$ of the double Fourier series:

$${}^t\ddot{W}_{rs}+\frac{K}{\rho h}\left(\frac{r^2\pi^2}{a^2}+\frac{s^2\pi^2}{b^2}\right)^2[{}^tW_{rs}-{}^0W_{rs}]-\frac{E}{\rho}\sum_{i=1}^{k}\sum_{j=1}^{l}\sum_{p=1}^{k}\sum_{q=1}^{l}(B_1+B_2)[{}^tW_{ij}^2$$

$$-{}^0W_{ij}^2]{}^tW_{pq}-\frac{E}{\rho}\sum_{i=1}^{k}\sum_{j=1}^{l}\sum_{m=1}^{k}\sum_{n=1}^{l}\sum_{p=1}^{k}\sum_{q=1}^{l}{}^{(i,j)\neq(m,n)}\{B_3+B_4+B_5+B_6\}[{}^tW_{ij}{}^tW_{mn}$$

$$-{}^0W_{ij}{}^0W_{mn}]{}^tW_{pq}+\frac{1}{\rho h}\frac{r^2\pi^2}{a^2}\bar{N}_x{}^tW_{rs}+\frac{1}{\rho h}\frac{s^2\pi^2}{b^2}\bar{N}_y{}^tW_{rs}$$

$$-\sum_{p=1}^{k}\sum_{q=1}^{l}\frac{8}{\rho h}\frac{pq\pi^2}{ab}XY(p,q,r,s)\bar{N}_{xy}{}^tW_{pq}=0, \tag{26}$$

$r=1, 2, \ldots, k$ respectively $s=1, 2, \ldots, l$.

The abbreviations B_1 to B_6 and XY are defined in Appendix A. The corresponding system of equations for static problems results from Eq. (26) by omitting ${}^t\ddot{W}_{rs}$. For dynamic buckling investigations q_z has not been considered.

A computer code that solves the dynamic problem in dependence on the imperfection coefficients ${}^0W_{mn}$ and the loading functions $\bar{N}_x(t)$, $\bar{N}_y(t)$ and $\bar{N}_{xy}(t)$ has been developed in FORTRAN. For time integration a fourth-order Runge–Kutta method has been used. The initial conditions are set as:

$${}^t\dot{W}_{mn}(t=0)=0 \tag{27}$$

and

$${}^tW_{mn}(t=0)={}^0W_{mn}. \tag{28}$$

To solve the coefficients of the deflection function in the static case, a quadratic convergent Newton method is applied.

Compared with calculations performed by the finite element code MSC-Nastran for static as well as for dynamic analysis, the applied Galerkin method is very effective in relation to deflection and stress analysis because only a few modes have to be employed for the investigations [8]. The CPU time increases nearly quadratically with the number of terms of the Fourier series.

5. Results and discussion

In this section results will be presented for aluminium alloy plates with various geometric dimensions and imperfections under unidirectional impact loading, $\bar{N}_x(t)$. In order to analyse the behaviour of dynamically loaded plates for different loading durations the amplitude of the loading function $\bar{N}_x(t)$, the exceeding of which leads to stress failure in the plate, is searched. This computation is performed by a bisection method which varies the pulse amplitude. For every bisection step the system of coupled differential equations (26) has to be solved. The effective stress σ_E is calculated by using the von Mises yield criterion [9]:

$$\sigma_E=\sqrt{\sigma_x^2+\sigma_y^2-\sigma_x\sigma_y+3(\tau_{xy}^2+\tau_{yz}^2+\tau_{xz}^2)}. \tag{29}$$

The results will be presented in form of DLF versus pulse duration (T_S) charts. To compute the DLF the static failure load, which is obtained by a static postbuckling calculation, is necessary. Unless otherwise stated, a one-term imperfection ${}^0W_{11}$, which corresponds to the basic buckling mode of the plates investigated, is used for the calculations. Because of the symmetric imperfection shape all antisymmetric terms of the Fourier series become zero. Therefore Navier's double series can be reduced to a summation over odd indices, and so the CPU time decreases considerably. The calculations, the results of which are presented in this paper, are performed by using a (k=5)×(l=3) series that results in convergent solutions.

5.1. Influence of pulse duration

The dependence of the dynamic behaviour of a structure on the pulse duration could be described by a shock spectrum. In such a chart the residual response amplitudes and maximax response amplitudes are plotted over the duration of impact. The residual response amplitude is defined by the free vibration amplitude after loading, while the maximax response amplitude results from the maximum of deflection during the motion of a structure caused by the loading [10]. For a sinusoidal impact function (S) that is described by

$$\bar{N}_x^S(t)=\begin{cases} N_x^{\max}\sin\dfrac{\pi t}{T_S}, & 0\le t\le T_S \\ 0, & \text{otherwise} \end{cases}, \tag{30}$$

the shock spectrum of a plate (a/b=1; h/b=0.005; ${}^0W_{11}/h$=0.2; σ_L=100 MPa) subjected to a loading amplitude of $N_x^{\max}=3N_{crit}$ is presented in Fig. 2, in which the mid-point transverse deflection has been normalized to the corresponding static deflection, w_{stat}.

It is shown in Fig. 2 that the maximum of response is reached for a shock duration close to the period time of transverse vibration, T_P. The DLF plot of the plate is shown in Fig. 3. Depending on the shock duration, this chart yields the factor by which to multiply the static failure load to obtain the dynamic failure load. Accordingly the DLF plot is useful to get the dynamic failure load from the corresponding static load. If the DLF plot is known, the design of plates relating to in-plane dynamic loading is reduced to a static postbuckling analysis. In design practice such computations are performed by the simple method of effective width [6].

As demonstrated in the plot, high loads are possible without the occurrence of failure for short-time pulses while for higher pulse durations — because of the dynamic overshooting of displacements — the dynamic load has to be reduced in relation to the static failure load.

For a wide range of shock durations loads smaller than the static failure load lead to stress failure in the plate. For high ratios of T_S/T_P the quasi-static limit load is reached asymptotically.

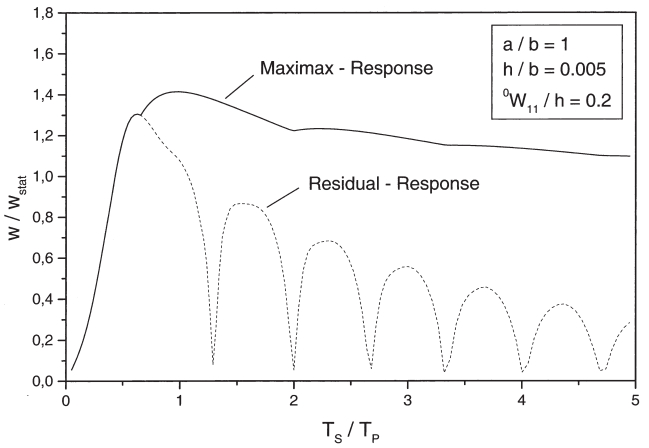

Fig. 2. Shock spectrum of a plate subjected to unidirectional dynamic loading ($N_x^{max}=3N_{crit}$).

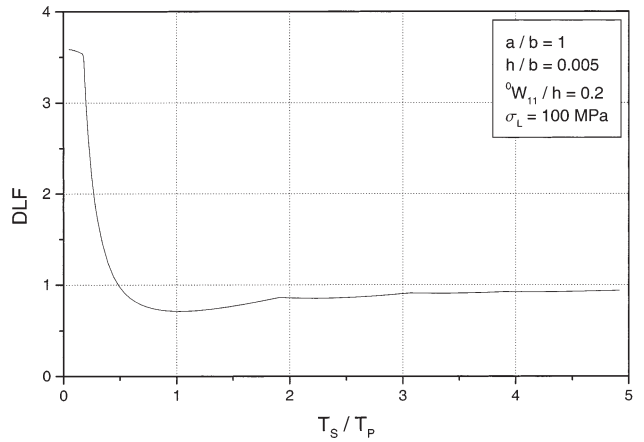

Fig. 3. DLF plot of a plate subjected to unidirectional dynamic loading.

As in the shock spectrum, the effects of transverse inertia affect the DLF chart differently depending on the pulse duration. The DLF plot corresponds with the shock spectrum. Thus high deflections in the shock spectrum result in low DLF values. On account of the non-linear behaviour, local maxima or minima in the DLF plot and the shock spectrum are not reached for exactly the same shock durations.

Fig. 3 also shows that the dynamic load-amplification factor is limited for short pulse durations by the flat plates problem:

$$\mathrm{DLF}_{\max}=\frac{\sigma_{\mathrm{L}}h}{|N_{\mathrm{F}}^{\mathrm{stat}}|}. \tag{31}$$

5.2. Influence of the shock function

To examine the influence of different loading functions on the dynamic behaviour of imperfect plates, in addition to the sinusoidial impact rectangular (R) and triangular (T) pulses will be investigated. These two functions are described by:

$$\bar{N}_x^{\mathrm{R}}(t)=\begin{cases} N_x^{\max}, & 0\le t\le T_{\mathrm{S}} \\ 0, & \text{otherwise} \end{cases} \tag{32}$$

and

$$\bar{N}_x^{\mathrm{T}}(t)=\begin{cases} 2N_x^{\max}\dfrac{t}{T_{\mathrm{S}}}, & 0\le t\le \dfrac{T_{\mathrm{S}}}{2} \\ 2N_x^{\max}\left(1-\dfrac{t}{T_{\mathrm{S}}}\right), & \dfrac{T_{\mathrm{S}}}{2}< t\le T_{\mathrm{S}} \\ 0, & \text{otherwise} \end{cases}. \tag{33}$$

The corresponding DLF plots (Fig. 4) show that the particular force function influences the dynamic behaviour of stability exceptionally.

In the region of residual response, which is characterized by the visible drop in DLF, the plot moves to shorter pulse durations for shock functions with higher pulse area (i.e., impulse) if the loading parameters (T_{S}, $N_x^{\max}$) are equal. In the same way the DLF reaches lower values. While shock functions having finite rise time — like the sinusoidial or the triangular pulse — approach quasi-static behaviour for higher shock durations, the rectangular pulse having infinite rise time is constant after reaching its minimum. It has been demonstrated that the position of the DLF plots to one another is defined by the impulse ratio of the shock functions which have equal loading parameters [11].

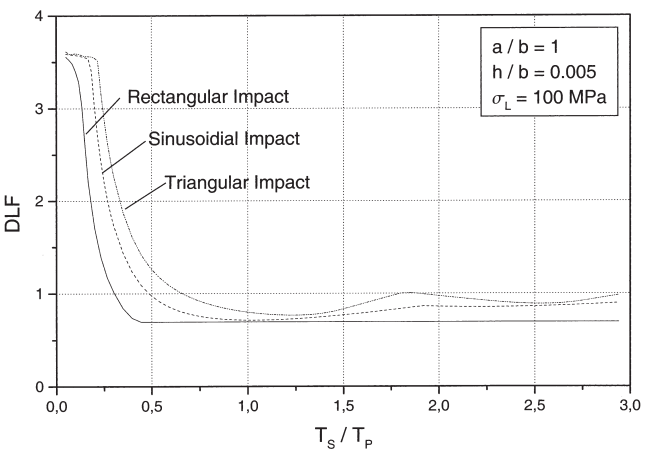

Fig. 4. Influence of the shock function on dynamic buckling.

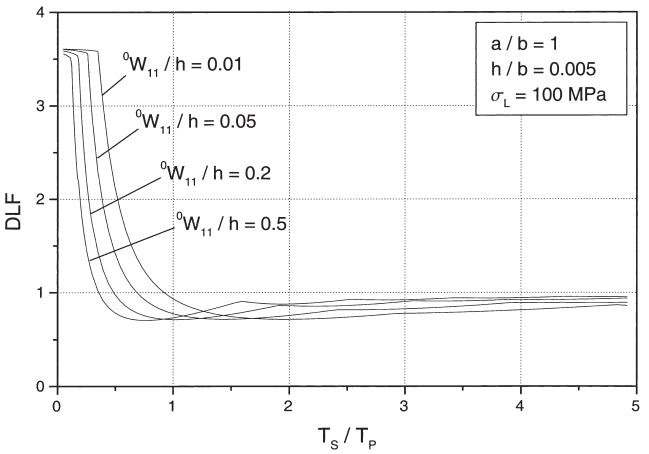

Fig. 5. DLF plots for different imperfection magnitudes.

5.3. Imperfection sensitivity

Many publications have been pointed out the imperfection sensitivity of dynamic stability behaviour [3,12]. The DLF plots of four plates having different geometric imperfections ($^0W_{11}/h$=0.01, 0.05, 0.2, 0.5) are compared in Fig. 5. As shown, higher imperfection leads to smaller dynamic load-amplification factors for short pulse durations while, for higher durations, the DLF of plates having minor imperfection is comparatively small. The smaller the magnitude of imperfection, the more the dynamic deflection lags behind the static one, which is shown in Fig. 6. This is why the location of the DLF minimum is dependent on the size of imperfection.

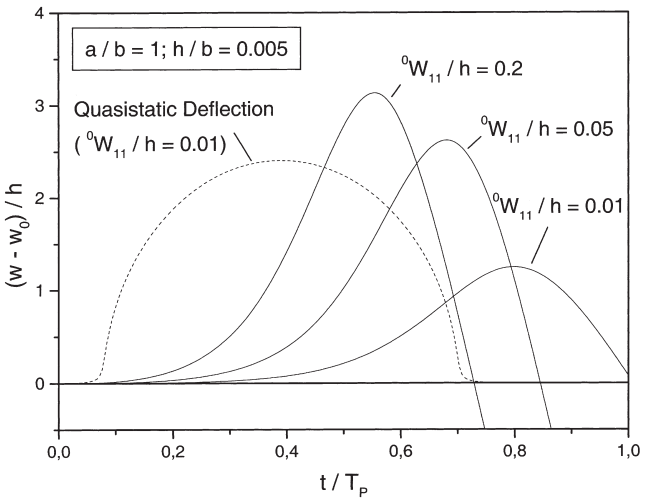

Fig. 6. Response curves for different imperfection magnitudes (T_S/T_P=0.78; N_x^{max}=0.7N_F^{stat}; σ_F=100 MPa).

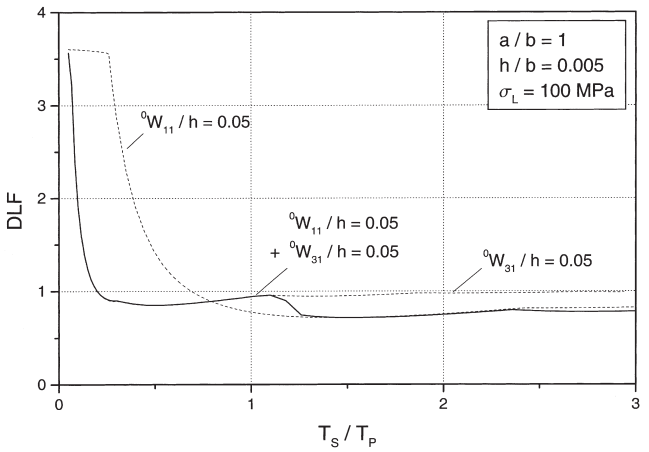

Fig. 7. Influence of geometric imperfection shapes on dynamic buckling.

In previous publications on plates subjected to in-plane pulse loading only one term of the imperfection function (22) has been considered. But if there exist more wave terms of imperfection, the dynamic behaviour of stability is influenced differently for varying pulse durations. Thus higher undulating imperfections influence the dynamic behaviour of short-duration impacts considerably, while for long-duration pulses imperfections of high wavelength dominate the plate's dynamic behaviour. Fig. 7 shows this effect of imperfection superposition.

5.4. Influence of geometric dimensions

DLF plots of three plates with different thickness (h/b=0.0025, 0.00375, 0.005) are demonstrated in Fig. 8. Because of the variable thickness also the $^0W_{11}/h$ ratio differs. All other plate parameters are identical.

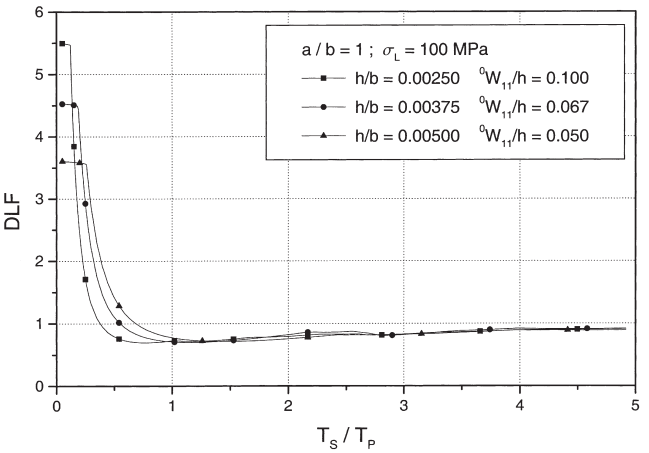

Fig. 8. Influence of the plate thickness on dynamic buckling.

For higher pulse durations the thickness of a plate does not affect its dynamic stability much. But there exist differences in dynamic behaviour for short-time impacts. Investigations proved that the influence of varying ${}^0W_{11}/h$ ratio is not responsible for the change in the DLF plot. The thinner the plates, the more the drop in DLF moves to shorter pulse durations. The thicker the plates, the more the dynamic deflections lag behind the quasi-static deflections (cf. influence of the magnitude of the imperfection).

The static failure load decreases overproportionally while the dynamic failure load falls proportionally by reducing the thickness [Eq. (31)], thus higher maxima of DLF are reached for thinner plates.

Fig. 9 shows three DLF plots of plates with the same static basic buckling mode. As demonstrated, the aspect ratio of the plate does not affect the dynamic stability much.

5.5. Influence of failure stress

Fig. 10 shows DLF charts of plates made of aluminium alloys that have the same mechanical properties but different limit stresses (AlMg 5454: σ_L=80 MPa; AlMg 5086: 100 MPa; AlMg 5083: 130 MPa). All plates show nearly the same dynamic behaviour of stability. There is only a difference for short pulse durations: because of the non-linear behaviour, raising the limit load of the material σ_L increases the static failure load underproportionally. Considering that for short-time impacts the dynamic failure load is proportional to σ_L [Eq. (31)], the DLF increases.

5.6. Influence of the criterion of stability

In this section an example is given to show how the dynamic buckling load is affected by the criterion of stability.

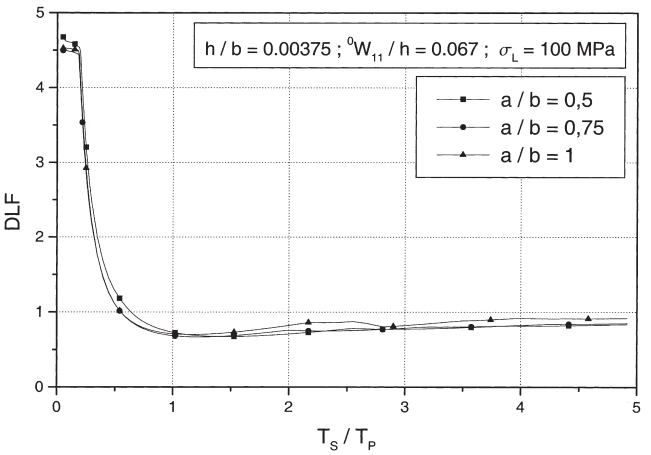

Fig. 9. DLF plots for different aspect ratios a/b.

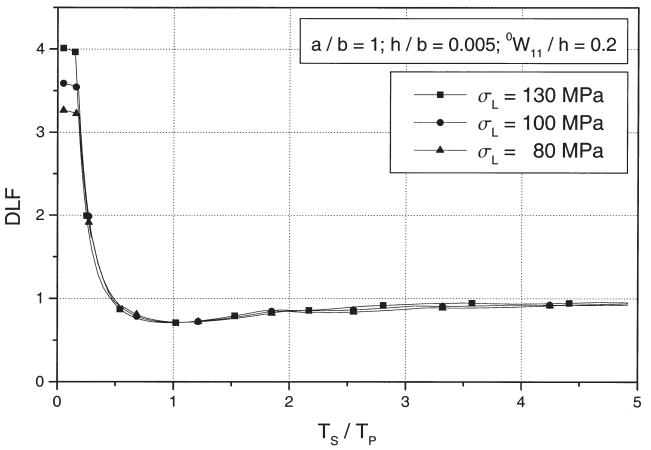

Fig. 10. Influence of the material's limit stress σ_F on dynamic buckling.

For a shock duration T_S/T_P=1, the dynamic buckling load is computed by the Budiansky–Hutchinson [1] criterion and the stress failure criterion (1). To determine the dynamic buckling load by the Budiansky–Hutchinson criterion [1], the maximum deflection in the *z*-direction caused by the impact is investigated by variation of the loading amplitude. The dynamic buckling load based on the Budiansky–Hutchinson criterion [1] is defined by the maximum of the gradient $\partial w_{max}/\partial N_x^{max}$. In Fig. 11 the corresponding dynamic buckling load and the region of instability are marked. The dynamic buckling load computed by the stress failure criterion applied in this paper is shown as well. Hence it appears in the example that the load-carrying capability is only exploited for nearly 50% by the Budiansky–Hutchinson criterion [1].

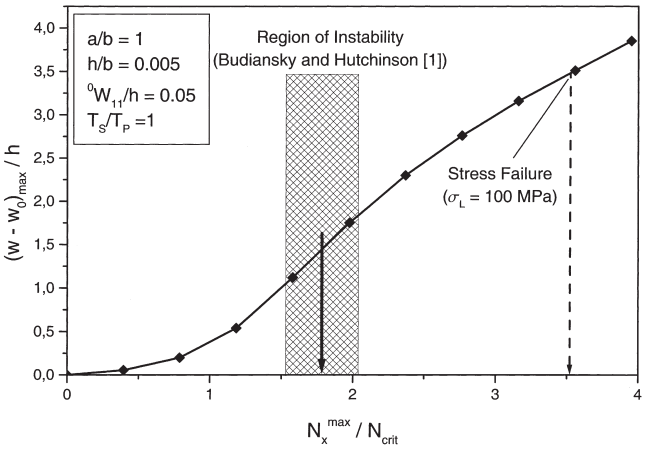

Fig. 11. Comparison of Budiansky–Hutchinson [1] and stress failure criteria.

6. Conclusions

A study of dynamic buckling of thin isotropic plates under unidirectional loading has been presented in this paper. For this purpose a stress failure criterion has been applied which considers the load-carrying capability of the structure. It has been demonstrated that application of the criterion of Budiansky and Hutchinson [1] is not suitable for the design of plates considering dynamic buckling in lightweight structures.

The dynamic load factor (DLF) has been defined such that it describes only dynamic effects in dependence on the shock duration. If the DLF is known, the design of plates relating to dynamic buckling is reduced to a non-linear static post-buckling analysis. For a wide range of shock durations DLFs smaller than unity are caused by the dynamic overshooting of the structure. As demonstrated in this paper, the dynamic behaviour of a plate subjected to in-plane dynamic loading is essentially influenced by the loading function, the duration of impact and the geometric imperfections. Not only the magnitude of the imperfection but also its shape affect dynamic buckling considerably. Regarding the variation of the other parameters (i.e., ultimate stress, thickness and aspect ratio), plates show only a modest sensitivity.

Appendix A

Shortenings $B_1, B_2, \ldots, B_6$ of Eq. (26):

$$B_1=\frac{i^2p^2\pi^4}{2a^4}X_1(p, r)Y_2(j, q, s),$$

$$B_2=\frac{j^2q^2\pi^4}{2b^4}X_2(i, p, r)Y_1(q, s),$$

$$B_3=\frac{(ijmn-i^2n^2)\pi^4}{[(i-m)^2b^2+(j-n)^2a^2]^2}\{[(j-n)^2p^2+(i-m)^2q^2]X_3(i, m, p, r)Y_3(j, n, q, s)-2(i-m)(j-n)pqX_4(i, m, p, r)Y_4(j, n, q, s)\},$$

$$B_4=\frac{(ijmn-i^2n^2)\pi^4}{[(i-m)^2b^2+(j+n)^2a^2]^2}\{[(j+n)^2p^2+(i-m)^2q^2]X_3(i, m, p, r)Y_5(j, n, q, s)-2(i-m)(j+n)pqX_4(i, m, p, r)Y_6(j, n, q, s)\},$$

$$B_5=\frac{(ijmn+i^2n^2)\pi^4}{[(i+m)^2b^2+(j-n)^2a^2]^2}\{[(j-n)^2p^2+(i+m)^2q^2]X_5(i, m, p, r)Y_3(j, n, q, s)-2(i+m)(j-n)pqX_6(i, m, p, r)Y_4(j, n, q, s)\}$$

and

$$B_6=\frac{(ijmn-i^2n^2)\pi^4}{[(i+m)^2b^2+(j+n)^2a^2]^2}\{[(j+n)^2p^2+(i+m)^2q^2]X_5(i, m, p, r)Y_5(j, n, q, s)-2(i$$

$$+m)(j+n)pqX_6(i, m, p, r)Y_6(j, n, q, s)\},$$

where $X_1, X_2, \ldots, X_6$ respectively $Y_1, Y_2, \ldots, Y_6$ and XY are defined by integrations of trigonometric functions:

$$XY(p, q, r, s)=\frac{1}{ab}\int_0^a\int_0^b \cos\frac{p\pi x}{a}\cos\frac{q\pi y}{b}\sin\frac{r\pi x}{a}\sin\frac{s\pi y}{b}\,\mathrm{d}x\,\mathrm{d}y,$$

$$X_1(p, r)=\frac{1}{a}\int_0^a \sin\frac{p\pi x}{a}\sin\frac{r\pi x}{a}\,\mathrm{d}x,$$

$$Y_1(q, s)=\frac{1}{b}\int_0^b \sin\frac{q\pi y}{b}\sin\frac{s\pi y}{b}\,\mathrm{d}y,$$

$$X_2(i, p, r)=\frac{1}{a}\int_0^a \cos\frac{2i\pi x}{a}\sin\frac{p\pi x}{a}\sin\frac{r\pi x}{a}\,\mathrm{d}x,$$

$$Y_2(j, q, s)=\frac{1}{b}\int_0^b \cos\frac{2j\pi y}{b}\sin\frac{q\pi y}{b}\sin\frac{s\pi y}{b}\,\mathrm{d}y,$$

$$X_3(i, m, p, r)=\frac{1}{a}\int_0^a \cos\frac{(i-m)\pi x}{a}\sin\frac{p\pi x}{a}\sin\frac{r\pi x}{a}\,\mathrm{d}x,$$

$$Y_3(j, n, q, s)=\frac{1}{b}\int_0^b \cos\frac{(j-n)\pi y}{b}\sin\frac{q\pi y}{b}\sin\frac{s\pi y}{b}\,\mathrm{d}y,$$

$$X_4(i, m, p, r)=\frac{1}{a}\int_0^a \sin\frac{(i-m)\pi x}{a}\cos\frac{p\pi x}{a}\sin\frac{r\pi x}{a}\,\mathrm{d}x,$$

$$Y_4(j, n, q, s)=\frac{1}{b}\int_0^b \sin\frac{(j-n)\pi y}{b}\cos\frac{q\pi y}{b}\sin\frac{s\pi y}{b}\,\mathrm{d}y,$$

$$X_5(i, m, p, r)=\frac{1}{a}\int_0^a \cos\frac{(i+m)\pi x}{a}\sin\frac{p\pi x}{a}\sin\frac{r\pi x}{a}\,\mathrm{d}x,$$

$$Y_5(j, n, q, s)=\frac{1}{b}\int_0^b \cos\frac{(j+n)\pi y}{b}\sin\frac{q\pi y}{b}\sin\frac{s\pi y}{b}\,dy,$$

$$X_6(i, m, p, r)=\frac{1}{a}\int_0^a \sin\frac{(i+m)\pi x}{a}\sin\frac{p\pi x}{a}\sin\frac{r\pi x}{a}\,dx$$

and

$$Y_6(j, n, q, s)=\frac{1}{b}\int_0^b \sin\frac{(j+n)\pi y}{b}\sin\frac{q\pi y}{b}\sin\frac{s\pi y}{b}\,dy.$$

References

[1] Budiansky B, Hutchinson JW. Dynamic buckling of imperfection-sensitive structures. In: Applied Mechanics Proceedings of the 11th International Congress of Applied Mechanics. Berlin: Springer, 1964. p. 636–51.

[2] Huyan X, Simitses G. Dynamic buckling of imperfect cylindrical shells under axial compression and bending moment. AIAA J 1997;35(8):1404–12.

[3] Ari-Gur J, Singer J, Weller T. Dynamic buckling of plates under longitudinal impact. In: TAE No. 430. Haifa: Technion Israel Institute of Technology, Department of Aeronautical Engineering, 1981.

[4] Ari-Gur J, Simonetta SR. Dynamic pulse buckling of rectangular composite plates. Composites, Part B 1997;28B:301–8.

[5] Ari-Gur J, Elishakoff I. Effects of shear deformation and rotary inertia on the pulse buckling of imperfect plates. In: Recent Advances in Structural Mechanics PVP-vol. 227/NE-vol. 7. ASME, 1991.

[6] Singer J, Arbocz J, Weller T. Buckling experiments: experimental methods in buckling of thin-walled structures. Chichester (UK): John Wiley & Sons, 1998.

[7] Wolmir AS. Biegsame Platten und Schalen. Berlin: VEB Verlag für Bauwesen, 1962.

[8] Petry D. Imperfekte isotrope Platten unter ebener Stoßbelastung (in German). Research Report 99-01. Munich: Universität der Bundeswehr München, Institut für Luftfahrttechnik und Leichtbau, 1999.

[9] Pilkey WD. Formulas for stress, strain, and structural matrices. New York: John Wiley & Sons, 1994.

[10] Harris CM, Crede CE. Shock and vibration handbook. 2nd ed. New York: McGraw-Hill, 1976.

[11] Petry D. Einfluss der Stoßfunktion auf das dynamische Stabilitätsverhalten von Platten unter ebener Impactbelastung (in German). In: Technical Note TN99-01. Munich: Universität der Bundeswehr München, Institut für Luftfahrttechnik und Leichtbau, 1999.

[12] Ekstrom RE. Dynamic buckling of a rectangular orthotropic plate. AIAA J 1973;11(12):1655–9.